Journal of Materials Chemistry C

ROYAL SOCIETY OF CHEMISTRY

PAPER

View Article Online
View Journal | View Issue

Cite this: J. Mater. Chem. C, 2025, 13, 20580

Maximizing sunlight absorption in narrow bandgap semiconducting copper(I) iodides for enhanced photocatalytic dye degradation

Gia M. Carignan,[a] Simon J. Teat,[b] Xiuze Hei,[c] Srinivas Chakravartula,[a] Gene Hall,[a] Le Hong Nguyen[a] and Jing Li *[ad]

Received 30th June 2025,
Accepted 8th September 2025

DOI: 10.1039/d5tc02511g

rsc.li/materials-c

Photocatalytic dye degradation leverages sunlight to break down dyes and pigments into safer, simpler molecules. Using a material that can absorb a broad range of the solar spectrum optimizes the speed and efficiency of this process. In this study, we explore a series of new, narrow bandgap copper iodide semiconductors (1.5–1.7 eV) with various dimensionalities (0D to 3D) to evaluate their photocatalytic efficiency in dye degradation. The most effective material achieved 95% degradation within just 27 minutes. Mass spectrometry provided a detailed insight and in-depth understanding into the degradation mechanism. All materials demonstrated excellent stability under ambient conditions, highlighting their promise as eco-friendly candidates for dye degradation in water purification.

Introduction

Organic dyes are widely used in the production of various commercial goods and, as a result, are frequently present in industrial wastewater. These dyes pose environmental concerns due to their toxicity and their ability to obstruct sunlight penetration, hindering photosynthetic organisms in aquatic systems.[1] Therefore, there is an urgency to develop photocatalysts that can break down these dyes in a sustainable and safe way. However, many organic dyes are both highly water-soluble and resistant to degradation by heat or oxidants, presenting a significant challenge. Traditional approaches, such as chemical and biological oxidation or adsorption, aim to completely remove these compounds from water.[2,3] However, in addition to being time consuming, these methods can be costly.[4] Photocatalytic degradation, on the other hand, offers a promising alternative by harnessing sunlight and utilizing a low-cost, eco-friendly photocatalyst to break down dyes into harmless byproducts.[5]

Copper(I) halide hybrid semiconductors have been intensively researched for the past few decades due to their impressive luminescence efficiency,[6–8] performance in a variety of applications,[9,10] and the interesting photophysical and structural characteristics that arise from their extremely diverse nature.[11–13] Copper(I) iodide (CuI) hybrid materials have also been shown as effective and efficient catalysts due to their transition metal centers,[14] while remaining cost-effective and eco-friendly in contrast to their noble metal counterparts (Pt(II), Au(III) and Ag(I)).[15–17] More specifically, CuI hybrids have also been used as photocatalysts for the degradation of common dyes such as methylene blue (MB) and rhodamine B.[4,18,19] However, their performance needs to be improved due to various issues such as extended degradation times and poor recyclability.[20,21]

Other, well established, photocatalysts such as TiO_2, CdS, AgI, CuS, *etc.* can, in some cases, degrade MB to the same extent as the present work.[22] However, these all-inorganic materials suffer in their practicality as they require high sintering temperatures for synthesis, utilize toxic, expensive or heavy metals, or need co-catalysts and/or modifications to achieve promising photocatalytic behavior.[23] When considering large scale production at the industrial level, CuI hybrids display significant advantages over other all-inorganic alternatives. Specifically, for example, TiO_2 requires calcination temperatures of over 600 °C for synthesis.[24] CdS and AgI contain elements that are hazardous and highly regulated. When considering all cost effects, CuI hybrid materials offer a less expensive option to other photocatalysts as their synthesis methods is more energy efficient and their reagents are readily available and inexpensive. Therefore, CuI hybrids are economically competitive for large-scale production.

Copper(I) hybrids can be grouped into three main classes: type-I, type-II and type-III, or all-in-one (AIO). Type-I refers to

[a] Department of Chemistry and Chemical Biology, Rutgers University, Piscataway, New Jersey 08854, USA. E-mail: jingli@rutgers.edu
[b] Advanced Light Source, Lawrence Berkeley National Laboratory, Berkeley, CA, 94720, USA
[c] Hoffman Institute of Advanced Materials, Shenzhen Polytechnic, 7098 Liuxian Blvd, Nanshan District, Shenzhen, 518055, China
[d] Department of Information Display, Kyung Hee University, 26 Kyungheedae-ro, Dongdaemun-gu, Seoul 02447, Republic of Korea

structures composed of CuI inorganic modules and organic ligands *via* coordinate bonds between Cu and N, or S. Type-II structures differ as their inorganic units are anionic, forming only ionic bonds with organic cations. Type-III (AIO-type) structures incorporate both coordinate and ionic bonds between the inorganic and organic units, therefore combining the structural features of type-I and type-II. They have been designed to realize the beneficial properties of both type-I and -II within one structure. These properties include a variety of emission colors, impressive photoluminescence quantum efficiency (PLQY), high thermal stability, robustness toward ambient conditions or water and high solubility for solution processability.[8,25,26]

The CuI inorganic modules and overall hybrid structures can vary in dimensionality, from 0D to 3D, and their photocatalytic performance may vary based on this since the amount of Cu can affect photocatalytic activity. Furthermore, since the degradation of dyes is sunlight driven, the ideal photocatalyst candidates will have narrow bandgaps, to maximize the absorption of the solar spectrum. With potential applications in photovoltaics, photocatalysis, and photodetection, this series of materials was intentionally designed to have narrow bandgaps. The tuning of bandgaps in CuI hybrids that undergo metal to ligand charge transfer (MLCT) process has been investigated in depth.[25,27–29] Guided by this designing principle, we have synthesized and structurally characterized a series of narrow bandgap AIO-type CuI hybrids, namely, 3D-Cu_8I_{12}(*pnbpz*)$_2$ (*pnbpz* = 1,1′-(pentane-1,5-diyl)bis(pyrazin-1-ium)) (**1**), 0D-Cu_3I_5(*pbpz*)(MeCN) (*pbpz* = 1,1′-(propane-1,3-diyl)bis(pyrazin-1-ium)) (**2**), 0D-Cu_3I_5(*bbpz*)(MeCN) (*bbpz* = 1,1′-(butane-1,3-diyl)bis(pyrazin-1-ium)) (**3**) and 1D-Cu_8I_{12}-(*ophpz*)$_2$ (*ophpz* = 1,1′-(1,2-phenylenebis(methylene))bis(pyrazin-1-ium)) (**4**), and tested their application as photocatalysts in the degradation of MB. Our results show that all four compounds are narrow bandgap semiconductors exhibiting efficient and fast photodegradation performance, impressive recyclability and water stability.

Results and discussion

Structural design and description

To maximize sunlight absorption, narrow bandgaps semiconductors are the most desirable candidate for photocatalyst materials. To ensure this, cationic pyrazine-based ligands were used in the synthesis due to their low-lying lowest unoccupied molecular orbital (LUMO) energy levels. As demonstrated in previous studies, theoretically calculating the LUMO energy of a ligand or cation can aid in the process of designing hybrid materials with targeted bandgaps.[30] Table S1 presents the relationship between LUMO energies of the ligands and bandgaps of the corresponding CuI hybrid compounds. The general molecular structures of these ligands are shown in Fig. 1a. Their synthesis protocols have not been reported previously. Their ^{1}H-NMR data can be found in Fig. S1. To obtain high quality single crystals suitable for single crystal X-ray diffraction (SCXRD), the layer diffusion method and the antisolvent assisted crystallization method were used[13,31] (Fig. S2). The crystal structures of compounds **1–4** are depicted in Fig. 1b–d and Fig. S2a–d. Direct coordination between cationic ligands at the nitrogen site and anionic CuI at Cu atoms produce a series of overall neutrally charged AIO-type materials.

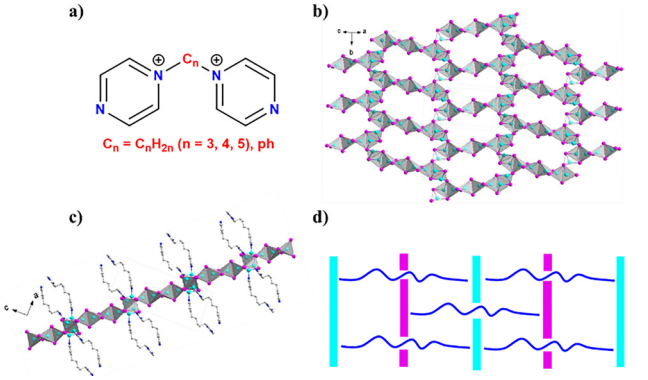

Fig. 1 (a) Structural depiction of pyrazine-based ligands. Crystal structure of 1; (b) view of one Cu_8I_{12} layer. (c) View down the *b*-axis of the Cu_8I_{12} layer and coordinated ligands. Color scheme: cyan: Cu; magenta: I; gray: C; blue: N. (d) Cartoon drawing of compound **1**'s interpenetrating structure. Cyan and magenta lines represent CuI sheets; blue curved lines represent coordinated ligands.

The crystal structure of compound **1** can be described as anionic 2D-$Cu_8I_{12}^{4-}$ layers connected by cationic $(pnbpz)^{2+}$ ligands to create an overall 3D structure (Fig. 1b and c). Furthermore, each ligand that connects two layers also interpenetrates through a third layer as depicted in Fig. 1d. To our knowledge, a 3D AIO-type structure of this type has never been reported before. This may be due to the structure-directing effect that arises from utilizing a flexible and long ligand with two coordinated N sites. Compounds **2** and **3** share the same Cu_3I_5 molecular modules, but ligands interact differently in each structure. Two open Cu sites are available for bonding with organic ligands in these cluster motifs. In compound **2**, one such site bonds to one ligand and the other, to an acetonitrile molecule (Fig. S2b). Note that only one N site on the *pbpz* ligand forms a bond with Cu, which could be due to the short alkyl chain creating steric hindrance, preventing the binding of second N. In Compound **3**, on the other hand, two Cu_3I_5 clusters each bind to one side of the two ligands *via* N atoms, creating a dimeric ring structure $(Cu_3I_5)_2$ (Fig. S2c). Compound **4** has a completely different structure, where large 0D-$Cu_8I_{12}^{4-}$ clusters are connected by *ophpz* ligands to form an overall 1D structure (Fig. S2d).

All Cu atoms in compounds **1–4** are tetrahedrally coordinated, while I atoms range from one to three coordination, as commonly observed in AIO-type structures.[10,32,33] They crystallize in space groups $P2_1/c$, $Pbca$, $P2_1/c$ and $C2/c$, respectively. More detailed crystallographic information can be found in Table S2, including the closest Cu···Cu and Cu···N distances which are similar to those of other reported AIO-type hybrid materials.[9,12,32] To confirm phase purity, powder X-ray diffraction (PXRD) patterns were collected on all samples and compared to simulated patterns generated from SCXRD data (Fig. S3a).

Table 1 Important properties of compounds **1–4**

Compound	E_g (eV)	λ_{em} (nm)	FWHM (nm)	T_d[a] (°C)	Solubility[b] (mg mL^{-1})
1	1.57	940	270	150	60
2	1.54	1000	260	100	120
3	1.47	970	320	100	80
4	1.37	1100	260	120	80

[a] Decomposition temperature. [b] Tested in DMSO at room temperature.

Photophysical and stability characterization

The photophysical properties of all title compounds were investigated using near-infrared (NIR) photoluminescence (PL) spectroscopy and diffuse reflectance spectroscopy. The quantitative details are outlined in Table 1. All compounds were excited at a wavelength of 440 nm and display emission in the NIR region of the electromagnetic spectrum. These observations are consistent with their narrow band gaps and dark black color. Their emission profiles are broad, which is commonly seen in NIR emitters.[34,35] They are also mostly asymmetric, arising from differences in vibronic level distributions between ground and excited states, which is a well-known phenomenon of the Franck–Codon principle[36,37] (Fig. 2a and Fig. S3b). Excitation-dependent PL spectra were also collected for each sample where the excitation wavelength ranged from 360–460 nm. In all cases, the maxima of emission energies remained unchanged, only the PL intensity (Fig. 2b and Fig. S4a–c). This is indicative that their emissions originate from a single excitation process. The bandgaps of the title compounds range between 1.3 to 1.6 eV and are in trend with their maxima of emission energies (Table 1 and Fig. 2c inset).

To further investigate their excitation process and mechanism, density functional theory (DFT) was employed to calculate the density of states (DOS) of compounds **1–4**. For all compounds, the valence band maximum (VBM) is mostly made up of the 3d and 5p atomic orbitals of Cu and I, respectively. The conduction band minimum (CBM) is composed primarily of the LUMO energy of ligands (N and C 2p atomic orbitals), which points towards metal/halide-to-ligand charge transfer [(M + X)LCT], a very common excitation process in AIO-type materials and is well studied.[38–41] This clearly shows why ligands with low-lying LUMO energy levels give rise to narrow bandgap hybrids (Table S1 and Fig. S5).

Finally, to test the materials' stability before subjecting them to dye degradation experiments, compound **1** was placed in water at room temperature for a period of 2 months. PXRD patterns before and after water exposure were essentially the same, demonstrating the robustness of these materials in water and their viability as a photocatalyst in wastewater treatment (Fig. S6b). Finally, thermal stability was also measured through thermogravimetric (TG) analysis (Fig. S6a). All compounds remain stable up to 100 °C.

Photocatalytic performance and mechanism

CuI hybrid materials have been utilized as photocatalysts for dye degradation, and it is known that due to their semiconducting nature, they indeed can phototactically degrade common dyes such as MB, among others.[42–44] However, as the wastewater containing these dyes persists in the environment and poses a harmful issue to people and ecosystems, materials with faster and more efficient degradation capabilities are needed. Since sun irradiation is the main energy source for photocatalytic degradation, narrow bandgap materials are chosen to maximize sunlight absorption (Fig. 2c).

Photocatalytic degradation was tested for all compounds, with compound **1** giving the best performance. The photocatalytic behavior of compound **1** is shown in Fig. 3a, where ~95% of the characteristic MB absorption peak at 664 nm is degraded after just 27 minutes. The other compounds (**2–4**) also show effective degradation of MB, reaching 73% to 98% in time spans of 30 to 60 minutes. These results clearly demonstrate the advantage of utilizing narrow bandgap hybrids to break down MB. Importantly, all three components are necessary for efficient photodegradation: compound **1**, H_2O_2, and sunlight as highlighted in control trials (Fig. 3b, c and Fig. S10). Interestingly, compound **4**, which has the lowest bandgap of 1.37 eV, can degrade MB by the highest percentage, reaching up to 98.6% (Fig. S7c), significantly higher than compounds **2** and **3** which are 73.4% and 84.1%, respectively (Fig. S7a and b).

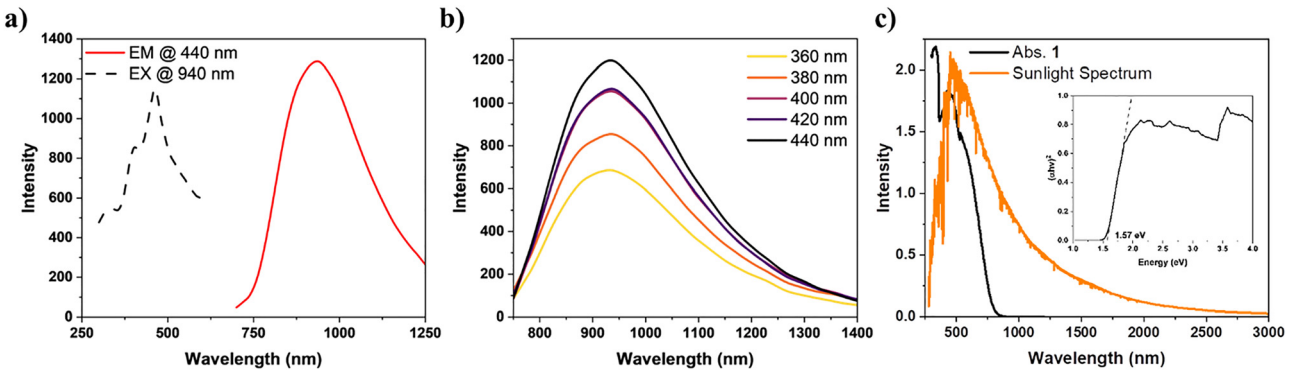

Fig. 2 (a) Excitation and emission spectra of compound **1**. (b) Excitation dependent PL spectra of compound **1**. (c) Optical absorption spectrum of compound **1** overlayed with the sunlight spectrum. Inset shows Tauc plot and estimated bandgap.

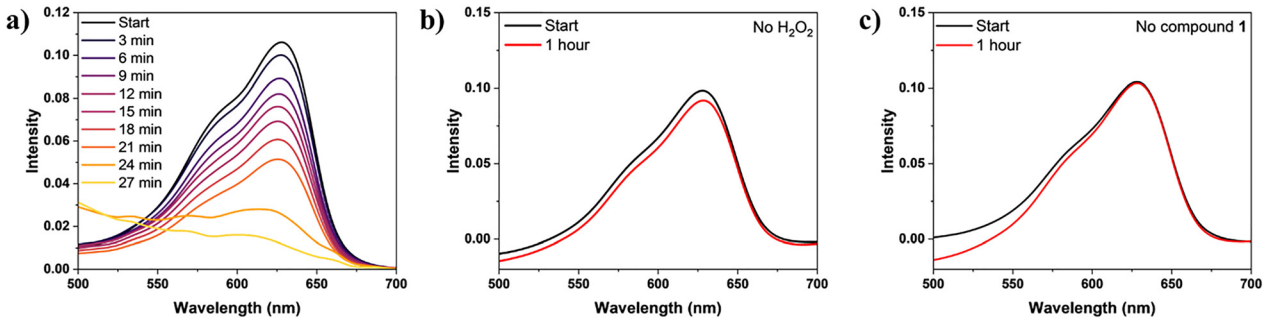

Fig. 3 Time dependent absorption spectra of MB solution during its photocatalytic degradation: (a) Compound **1** used as photocatalyst with H_2O_2. (b) Control trial without H_2O_2. (c) Control trial without compound **1**. For each experiment, a 10 ppm aqueous solution was used, along with 5 mg of compound **1** and 0.2 mL of H_2O_2 unless specified otherwise.

However, compound **4** takes almost double the amount of time to reach its degradation maximum. From the present work, it seems that higher dimensional structures (3D) with larger CuI ratios, and therefore more metal sites, such as compound **1**, may perform best in terms of photocatalytic efficiency and avoid certain trade-offs. With this hypothesis in mind, a reported 1D-AIO hybrid, 1D-$Cu_4I_6(btmmp)_2$,[45] with band gap of 2.5 eV was also tested with the same experimental conditions (Fig. S9). After 30 minutes, MB was only degraded by a small amount. After 1 day, the maximum degradation was about 34%, further providing evidence that among AIO materials, higher dimensionality and lower band gap may enhance photocatalytic performance.

Recyclability was also investigated for compound **1** through repeated trials and PXRD. Since these hybrids are water-stable and the degradation process is not destructive, each sample can be used multiple times. This is especially important for practical applications in large wastewater volumes. The same 5 mg sample of compound **1** was recycled for five trials. After each 27-minute period, the absorption of MB solution was taken, as well as the PXRD of filtered compound **1** to check for any crystallinity loss. After five trials, degradation decreased by only 5% and all major peaks in the PXRD remained intact with similar intensity (Fig. 4a, b and Fig. S8a–e). This confirms the structural integrity and robustness of CuI hybrids.

To fully understand the mechanism of photocatalysis of the title compounds, known radical scavengers, along with compound **1** and H_2O_2, were added to a separate round of trials to test how they affect the degree of degradation. Absorption spectra were taken before and after one hour in these trials. Scavengers included benzoquinone (BQ), disodium ethylenediaminetetraacetic acid (Na_2EDTA) and isopropyl alcohol (IPA) for the capture of superoxide ($^{\bullet}O_2^-$), holes (h^+) and hydroxyl radicals, respectively.[46,47] Fig. 4c shows the absorption spectra from these experiments. The addition of EDTA and IPA significantly impedes degradation, with only ~40% of MB decomposing in these trials. However, when BQ is added, degradation proceeds smoothly without interference from the scavenger. In this case, the absorption trace shows an increase of around 500 nm due to BQ's dark color, while the 663 nm peak for MB disappears, confirming its degradation. This behavior with scavengers aligns with previous findings.[4,19] A photocatalytic reaction mechanism can be ascertained from this information, as shown in Fig. 5a. As established in many instances,[48–51] sunlight exposure causes the absorption of photons and separation of electron/hole pairs in which the electrons move from the VB to the CB. When H_2O_2 is present, it utilizes these electrons to make hydroxyl radicals and ions. These radicals are the key players in MB degradation, breaking it down into less harmful products. In the meantime, the holes also play a role,

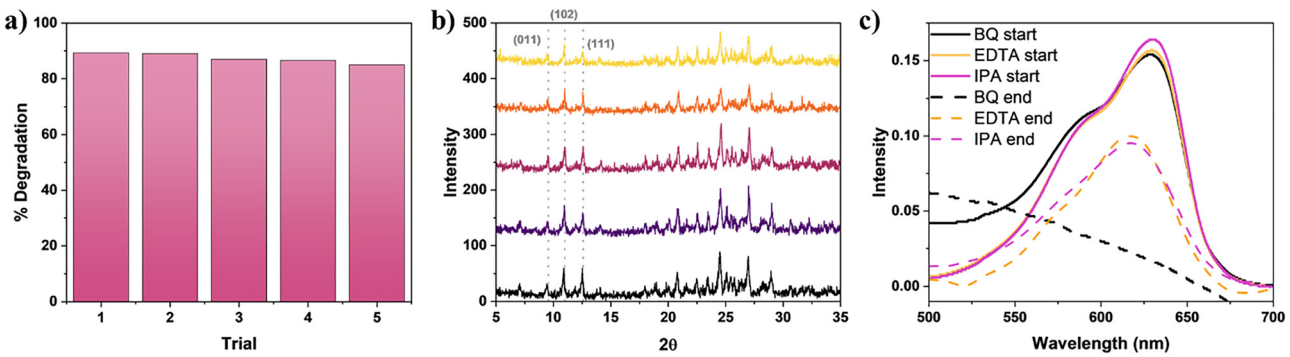

Fig. 4 (a) Percentage (%) degradation after multiple trials of the same sample of compound **1**. (b) PXRD patterns of the same sample of compound **1** after the completion of each degradation trial. (c) Absorption spectra of MB before and after degradation with compound **1** and various radical scavengers. For each experiment, a 10 ppm aqueous solution was used, along with 5 mg of compound **1**, 0.2 mL of H_2O_2 and 5 mg of selected scavenger.

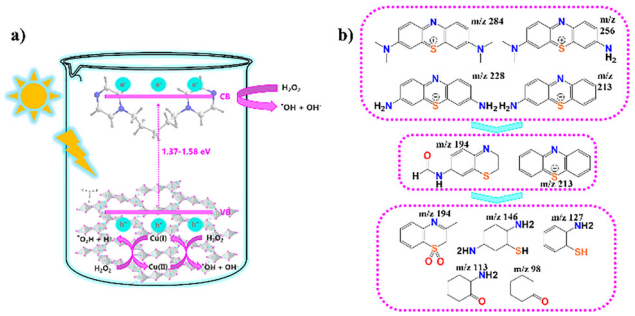

Fig. 5 (a) Schematic representation of excitation and degradation mechanism using compound **1** with H_2O_2. (b) Possible degradation products based on mass spectrometry results.

facilitating a Cu(I)/Cu(II) redox event, further producing hydroxyl radicals which break down MB further.

Furthermore, the products that MB decomposes into are also of interest, since these materials will then be present in the water supply. LC-MS analysis was performed on both a 10-ppm aqueous solution of MB before and after degradation to determine degradation products (Fig. S11 and S12). Possible degradation products are depicted in Fig. 5b and Fig. S12c. These are similar to other reported fragments and mechanisms, with small differences based on each photocatalyst.[52–54] There are many possible mechanisms based on the fragmentation results, but it can be said with certainty that MB no longer exists in the reaction solution since characteristic fragments of MB with *m*/*z* 284 and 312 ions disappeared while much lower weight fragments appeared (Fig. S13). We also confirmed through X-ray fluorescence (XRF) analysis that there was no change in the amount of Cu in the reaction solution post-degradation. Fig. S14 shows XRF analysis of both high-purity water and post-degradation solution in that same water. Cu, Ni, Ca and Fe were detected in both experiments with negligible differences based on the standard deviation and $<5\%$ error of the instrument, confirming there was no leeching of the photocatalyst into the reaction solution during photodegradation.

To further assess the practicality and usefulness of this material, a supplemental experiment was carried out for another common and more dangerous pollutant, phenol. With all other experimental parameters kept constant, compound **1** successfully degraded phenol by $\sim$53% after one hour when monitoring it's characteristic peak at 270 nm[55] (Fig. S15). Although not to the same extent as MB, this result shows compound **1** and other similar CuI hybrid materials may have promise as photocatalysts for degradation of a variety of common pollutants in wastewater. In comparison to other copper(I) hybrids, compound **1** performs extremely well towards MB, as it is the most efficient photocatalyst in this group and performs competitively among other hybrid and all-inorganic materials (Fig. S16 and Table S3).

Conclusion

A series of new CuI-based hybrid semiconductors with narrow bandgaps were synthesized and characterized, with their dimensionalities ranging from 0D to 3D. These compounds act as effective photocatalysts for the degradation of low-concentration MB in wastewater. These materials displayed strong absorption across the solar spectrum, accelerating the degradation rate and achieving up to 95% dye breakdown within 27 minutes for the most efficient compound. Mass spectrometry offered detailed insights into degradation mechanisms and byproducts, confirming both the high efficiency and the environmentally safe nature of this approach. These materials also demonstrated robust stability and recyclability under ambient conditions. Collectively, these findings establish that tuning and narrowing the bandgap of CuI hybrid semiconductors can yield highly promising, eco-friendly candidates for sustainable water purification through photocatalytic dye degradation.

Experimental

Materials

Pyrazine (99%, Matrix Scientific); 1,5-diiodopentane (97%, Thermo Scientific); 1,3-diiodopropane (98%, Ambeed Inc.); 1,4-diiodobutane (99%, Thermo Scientific); α,α′-dichloro-*o*-xylene (98%, TCI); sodium iodide (99%, VWR); potassium iodide (99%, Alfa Aesar); potassium carbonate (99%, TCI); dichloromethane (99%, VWR); acetone (99.5%, VWR); methanol (99%, VWR); dimethyl sulfoxide (99%, Beantown chemical); *N*,*N*-dimethylformamide (99%, VWR); acetonitrile (99.5%, VWR); ethyl acetate (99%, VWR); copper iodide (98%, Alfa Aesar); hydrogen peroxide (30%, VWR); benzoquinone (98.5, Thermo Scientific); disodium EDTA (0.5 M, VWR); isopropyl alcohol (99%, VWR).

Preparation of *pnbpz* I

Pyrazine (0.99 g, 12 mmol) was dissolved in 20 mL of acetonitrile at room temperature in a round bottom flask. 1,5-Diiodopentane (0.46 mL, 3 mmol) was added dropwise. The mixture was then stirred and heated to reflux for 12 hours. The reaction mixture was then subjected to rotary evaporation until only a small amount of acetonitrile remained. Ethyl acetate was added to fully precipitate the product which was then filtered and washed with ethyl acetate. The yield of the bright yellow product was 92%.

Preparation of *pbpz* I

A similar procedure to that of *pnbpz* I was used except 1,3-diiodopropane (0.39 mL, 3 mmol) was used. A bright yellow product was obtained, and the yield was 90%.

Preparation of *bbpz* I

A similar procedure to that of *pnbpz* I was used except 1,4-diiodobutane (0.45 mL, 3 mmol) was used. A bright yellow product was obtained, and the yield was 90%.

Preparation of *ophpz* I

α,α′-Dichloro-*o*-xylene (1.4 g, 8 mmol) was dissolved in acetone in a round bottom flask. A large excess of NaI (6.8 g, 45 mmol)

was added and the solution was heated to reflux for 12 hours. After cooling, the salt precipitate was filtered off and the filtrate was dried under vacuum. The residue was then dissolved in dichloromethane and extracted with water. The organic layer was then extracted with a saturated NaCl (brine) solution. The solvent was then removed under vacuum to give α,α′-diiodo-*o*-xylene. 2.5 g of this product was then dissolved into acetonitrile and an excess of pyrazine (1.2 g, 15 mmol) was added. This mixture was heated to reflux for 12 hours, and the reaction was then filtered to afford a dark yellow product. The yield of the final step is 83%.

Synthesis of compound 1

The layer diffusion method was used. 2 mmol of CuI was dissolved in 2 mL saturated potassium iodide solution. On top of this solution, 2 mL acetonitrile was slowly added as a buffer layer. Finally, 0.5 mmol of *pnbpz* I was dispersed in methanol and added as the top layer. After three days at 60 °C, black rod-shaped crystals were obtained in 45% yield based on CuI.

Synthesis of compound 2

A very similar procedure to that of compound **1** was used. Black block crystals were obtained in 52% yield based on CuI.

Synthesis of compound 3

The antisolvent assisted crystallization method was used in this case. 0.25 mmol of *bbpz* I and 1 mmol of CuI were dissolved in 1 mL of dimethyl sulfoxide in a small vial. This vial was placed inside a 20 mL vial filled with 5 mL acetonitrile antisolvent and placed in the 60 °C oven. Black block crystals were obtained in 39% yield based on CuI after 5 days.

Synthesis of compound 4

A similar procedure to that of compound **3** except *N*,*N*-dimethylformamide was used instead of dimethyl sulfoxide. Small black rod crystals were obtained in 55% yield based on CuI after 1 week.

Characterizations

Single crystal X-ray diffraction (SCXRD) was performed using a D8 goniostat equipped with a Bruker PHOTON100 CMOS detector at the Advanced Light Source (ALS) using synchrotron radiation. The structures were solved by direct methods and refined by full-matrix least-squares on F2 using the Bruker SHELXTL package.[56] The structures were deposited in Cambridge Crystallographic Data Center (CCDC) with numbers 2411484–2411487. Powder X-ray diffraction (PXRD) analysis was carried out on a Rigaku Ultima-IV unit using Cu Kα1 radiation (λ = 1.5406 Å) and a scan speed of 2° min^{-1}. Thermogravimetric analysis (TGA) was performed using the TA Instrument Q5000IR thermogravimetric analyzer with nitrogen flow and sample purge rates at 10 and 25 mL min^{-1}, respectively. Optical absorption spectra were measured at room temperature on a Shimadzu UV-3600 UV-vis–NIR spectrometer. The reflectance data were converted to Kubelka–Munk function. The data was further converted into a Tauc plot for bandgap determination.[57] Room temperature PL measurements were carried out on a FLS1000 spectrofluorometer (Edinburgh Instruments).

Liquid chromatography and mass spectrometry (LC-MS)

Reverse phase liquid chromatography (RPLC) was performed on Acquity UPLC, BEHC18,1.7 micron (2.1 × 50 mm) column Waters Corporation Inc. Column temperature was set at 40 °C. The following mobile phases were used: A: Water (HPLC grade) with 0.1% formic acid (MS grade); B: acetonitrile (HPLC grade) with 0.1% formic acid. The UPLC H-Class high flow LC (Waters Instruments) was operated at a flow rate of 0.4 mL min^{-1}, and 3 μL of sample was injected with an autosampler temperature maintained at 10 °C. For the separation of compounds, the following gradient concentrations was used starting with 5–95% B for 3.5 minutes and later to 5% B from 3.5–5 min. For column equilibration. Total run time of the LC-MS run was set for 5 minutes. ESI-MS experiments were performed on high resolution mass spectrometer (HRMS) in a sensitivity mode using a quadrupole-TOF hybrid mass spectrometer (Xevo-G2-XS-Q-tof: Waters Corp., Manchester, UK) in positive ionization mode with *m*/*z* scan range 100–2000. The applied experimental parameters were capillary voltage, 3.16 kV; sampling cone voltage, 30 V; source offset 60 °C; source temperature, 125 °C; desolvation temperature 300 °C: cone gas 25 L h^{-1} and desolvation gas 600 L h^{-1}. Data analysis was performed using Mass Lynx 4.1.

X-ray fluorescence (XRF)

A Horiba MESA-50 K energy dispersive X-ray fluorescence (EDXRF) spectrometer was used to measure the Cu concentration in a 400-μL aqueous solution after dye degradation experiment. The solution was transferred to an XRF cup equipped with a four-micron-thin Mylar window. Ultrapure water (18 megohm) from a Milli-Q Water System served as a blank for comparison with the analyzed samples.

The operating conditions of the spectrometer equipped with a Pd X-ray tube were as follows: 50 kV, 24 μA, 300-second acquisition time. Horiba XRF software was used to determine the peak area of the Cu 8.04 keV K-alpha X-ray. The detection limit for Cu under these operating conditions was 1 μg mL^{-1} (1 ppm). Peak intensities are determined through peak area integration. Concentration is not absolute but rather a relative amount based on a total of 100%. The software also corrects each peak based on the elements' inherent differences in cross-section area when evaluating the peak intensity.

Density functional theory (DFT)

The density of states (DOS) of selected compounds were calculated using the Cambridge Serial Total Energy Package (CASTEP).[58] Generalized gradient approximation (GGA) with Perdew–Burke–Ernzerhof (PBE) exchange correlation functional (XC) was used for all calculations. Ultrasoft pseudopotentials were used for all elements; the plane-wave kinetic cutoff and the total energy tolerance were set to be 351 eV

and 1×10^{-5} eV per atom, respectively. The *k*-point mesh used for compounds **1–4** were $7 \times 8 \times 3$, $4 \times 5 \times 4$, $7 \times 4 \times 3$ and $8 \times 8 \times 3$. All energy level calculations were based on Gaussian 09 with B3LYP hybrid functional and 6-311++G(3df,3pd) basis set. A frequency calculation was always performed after geometry optimization of all ligand molecules to confirm that the calculations resulted in a true minimum.

Photocatalytic experiments

Aqueous solutions of 10 ppm MB were prepared. 100 mL of this solution was used for each experiment in a beaker. The MB solution was wrapped in aluminum foil at first to keep out any sunlight. Hydrogen peroxide (0.2 mL) was added along with 5 mg of the selected hybrid compound. This mixture was stirred in darkness for 10 minutes to full combine before being placed in direct sunlight. The absorption of the solution was measured at three-minute intervals using a Shimadzu UV-3600 UV-vis–NIR spectrometer until the completion of the degradation process.

Author contributions

G. M. C.: methodology, investigation, formal analysis, visualization, and writing – original draft; S. J. T.: investigation (single-crystal); X. H.: temperature dependent photoluminescence measurements; S. C.: mass spectrometry measurements and analysis (advanced mass spectrometry facility); G. H.: X-ray fluorescence measurements and analysis; L. H. N.: methodology, investigation; J. L.: conceptualization, supervision, validation, and writing – review & editing.

Conflicts of interest

There are no conflicts to declare.

Data availability

All data supporting this research (including DFT, PL, PXRD, TGA, UV-vis, mass spectrometry *etc.*) are included in the main article and/or SI. Experimental details, PXRD, PL, TGA, UV-vis, mass spectrometry, X-ray fluorescence, theoretical calculation as well as crystal structure and single crystal data. See DOI: **https://doi.org/10.1039/d5tc02511g**.

CCDC 2411484–2411487 contain the supplementary crystallographic data for this paper.[59a–d]

Acknowledgements

The authors acknowledge the support from the U.S. Department of Energy, Office of Science, Office of Basic Energy Sciences (Grant No. DE-SC0019902). This research used the Advanced Light Source (ALS), which is a DOE Office of Science User Facility under Contract No. DE-AC02-05CH11231. G. M. C. also acknowledges the support of the Department of Defense through the National Defense Science and Engineering Graduate (NDSEG) fellowship program.

Notes and references

1 Y. Gao, S.-Q. Deng, X. Jin, S.-L. Cai, S.-R. Zheng and W.-G. Zhang, The construction of amorphous metal-organic cage-based solid for rapid dye adsorption and time-dependent dye separation from water, *Chem. Eng. J.*, 2019, **357**, 129–139.
2 D. Zhang, T. K. Ronson, Y.-Q. Zou and J. R. Nitschke, Metal–organic cages for molecular separations, *Nat. Rev. Chem.*, 2021, **5**(3), 168–182.
3 G. Boczkaj and A. Fernandes, Wastewater treatment by means of advanced oxidation processes at basic pH conditions: A review, *Chem. Eng. J.*, 2017, **320**, 608–633.
4 D. Pandey, A. Mishra, L. S. Kharabe, S. K. Maurya and A. Raghuvanshi, Semiconducting Copper(I) Iodide 2D-Coordination Polymers for Efficient Sunlight-Driven Photocatalysis in Dye Degradation, *Cryst. Growth Des.*, 2024, **24**(14), 6051–6059.
5 S. Frindy and M. Sillanpää, Synthesis and application of novel α-Fe2O3/graphene for visible-light enhanced photocatalytic degradation of RhB, *Mater. Des.*, 2020, **188**, 108461.
6 A. Y. Baranov, M. I. Rakhmanova, X. Hei, D. G. Samsonenko, D. V. Stass and I. Y. Bagryanskaya, *et al.*, A new subclass of copper(i) hybrid emitters showing TADF with near-unity quantum yields and a strong solvatochromic effect, *Chem. Commun.*, 2023, **59**(20), 2923–2926.
7 K. Zhu, Z. Cheng, S. Rangan, M. Cotlet, J. Du and L. Kasaei, *et al.*, A New Type of Hybrid Copper Iodide as Nontoxic and Ultrastable LED Emissive Layer Material, *ACS Energy Lett.*, 2021, **6**(7), 2565–2574.
8 X. Hei and J. Li, All-in-one: a new approach toward robust and solution-processable copper halide hybrid semiconductors by integrating covalent, coordinate and ionic bonds in their structures, *Chem. Sci.*, 2021, **12**(11), 3805–3817.
9 Y. V. Demyanov, Z. Ma, Z. Jia, M. I. Rakhmanova, G. M. Carignan and I. Y. Bagryanskaya, *et al.*, Copper(I)-Arsine Clusters with a Near-Unity Phosphorescence Quantum Yield for X-Ray Scintillation and LED Applications, *Adv. Opt. Mater.*, 2024, **12**(14), 2302904.
10 Z.-F. Wu, C. Wang, X. Liu, K. Tan, Z. Fu and S. J. Teat, *et al.*, Confinement of 1D Chain and 2D Layered CuI Modules in K-INA-R Frameworks via Coordination Assembly: Structure Regulation and Semiconductivity Tuning, *J. Am. Chem. Soc.*, 2023, **145**(35), 19293–19302.
11 G. M. Carignan, S. J. Teat, X. Hei and J. Li, Design, synthesis, structure analysis and photophysical characterization of robust and solution-processable one-dimensional copper(I) iodide-based inorganic-organic hybrid semiconductors, *J. Lumin.*, 2024, **269**, 120435.
12 X. Hei and J. Li, Making coordination networks ionic: a unique strategy to achieve solution-processable hybrid semiconductors, *Mater. Chem. Front.*, 2023, **7**(20), 4598–4604.
13 X. Hei, S. J. Teat, M. Li, M. Bonite and J. Li, Solution-Processable Copper Halide Based Hybrid Materials Consisting of Cationic Ligands with Different Coordination Modes, *Inorg. Chem.*, 2023, **62**(8), 3660–3668.

14 A. L. Stein, D. Alves, J. T. da Rocha, C. W. Nogueira and G. Zeni, Copper iodide-catalyzed cyclization of (Z)-chalcogenoenynes, *Org. Lett.*, 2008, **10**(21), 4983–4986.
15 C. E. Strasser and V. J. Catalano, ''On−Off'' Au(I)···Cu(I) Interactions in a Au(NHC)2 Luminescent Vapochromic Sensor, *J. Am. Chem. Soc.*, 2010, **132**(29), 10009–10011.
16 M. Yasui, K. Sakamoto, A. Ichimonji, N. Takeda and M. Ueda, Gold(III)-Catalyzed Cyclization/Skeletal Rearrangement Reaction for the Synthesis of 2,4,6-Trisubstituted 3-Hydroxypyridines, *ChemistrySelect*, 2024, **9**(38), e202403541.
17 X.-W. Lei, C.-Y. Yue, J.-Q. Zhao, Y.-F. Han, J.-T. Yang and R.-R. Meng, *et al.*, Two Types of 2D Layered Iodoargentates Based on Trimeric [Ag3I7] Secondary Building Units and Hexameric [Ag6I12] Ternary Building Units: Syntheses, Crystal Structures, and Efficient Visible Light Responding Photocatalytic Properties, *Inorg. Chem.*, 2015, **54**(22), 10593–10603.
18 M. Murillo, R. Wannemacher, J. Cabanillas-González, U. R. Rodríguez-Mendoza, J. Gonzalez-Platas and A. Liang, *et al.*, 2D Cu(I)-I Coordination Polymer with Smart Optoelectronic Properties and Photocatalytic Activity as a Versatile Multifunctional Material, *Inorg. Chem.*, 2023, **62**(28), 10928–10939.
19 P. Tang, X.-X. Xie, Z.-Y. Huang, Z.-Y. Kuang, S.-L. Cai and W.-G. Zhang, *et al.*, Two Cu(i) coordination polymers based on a new benzimidazolyl-tetrazolyl heterotopic ligand for visible-light-driven photocatalytic dye degradation, *CrystEngComm*, 2023, **25**(3), 417–424.
20 X.-S. Zhang, J.-L. Cui, Y. Liu, W.-Z. Li, Y. Liu and H. Xiang, *et al.*, Influence of anions on the synthesis of Cu(i)-based coordination polymers along with a series of derived materials for selective photocatalytic properties, *Mol. Syst. Des. Eng.*, 2023, **8**(11), 1388–1401.
21 C. Xu, W. Chen, J. Wang, Q. Wu, P. Wu and L. Tang, Two Cu(I\II) Coordination Polymers for Photocatalytic Degradation of Organic Dyes and Efficient Detection of Fe3+ Ions, *J. Inorg. Organomet. Polym. Mater.*, 2023, **33**(4), 885–894.
22 C. Sahoo, A. K. Gupta and I. M. Sasidharan Pillai, Photocatalytic degradation of methylene blue dye from aqueous solution using silver ion-doped TiO_2 and its application to the degradation of real textile wastewater, *J. Environ. Sci. Health, Part A: Toxic/Hazard. Subst. Environ. Eng.*, 2012, **47**(10), 1428–1438.
23 H. Wang, D. Zhou, S. Shen, J. Wan, X. Zheng and L. Yu, *et al.*, The photocatalytic activity and degradation mechanism of methylene blue over copper(ii) tetra(4-carboxyphenyl) porphyrin sensitized TiO2 under visible light irradiation, *RSC Adv.*, 2014, **4**(55), 28978–28986.
24 H. H. Shaarawy, H. S. Hussein, N. H. Hussien, G. A. Al Bazedi and S. I. Hawash, Green production of titanium dioxide nanometric particles through electrolytic anodic dissolution of titanium metal, *Environ. Sci. Pollut. Res. Int.*, 2023, **30**(9), 24043–24061.
25 W. Liu, K. Zhu, S. J. Teat, G. Dey, Z. Shen and L. Wang, *et al.*, All-in-One: Achieving Robust, Strongly Luminescent and Highly Dispersible Hybrid Materials by Combining Ionic and Coordinate Bonds in Molecular Crystals, *J. Am. Chem. Soc.*, 2017, **139**(27), 9281–9290.
26 X. Hei, W. Liu, K. Zhu, S. J. Teat, S. Jensen and M. Li, *et al.*, Blending Ionic and Coordinate Bonds in Hybrid Semiconductor Materials: A General Approach toward Robust and Solution-Processable Covalent/Coordinate Network Structures, *J. Am. Chem. Soc.*, 2020, **142**(9), 4242–4253.
27 Y. Fang, W. Liu, S. J. Teat, G. Dey, Z. Shen and L. An, *et al.*, A Systematic Approach to Achieving High Performance Hybrid Lighting Phosphors with Excellent Thermal- and Photostability, *Adv. Funct. Mater.*, 2017, **27**(3), 1603444.
28 X. Zhang, W. Liu, G. Z. Wei, D. Banerjee, Z. Hu and J. Li, Systematic Approach in Designing Rare-Earth-Free Hybrid Semiconductor Phosphors for General Lighting Applications, *J. Am. Chem. Soc.*, 2014, **136**(40), 14230–14236.
29 W. Liu, Y. Fang, G. Z. Wei, S. J. Teat, K. Xiong and Z. Hu, *et al.*, A Family of Highly Efficient CuI-Based Lighting Phosphors Prepared by a Systematic, Bottom-up Synthetic Approach, *J. Am. Chem. Soc.*, 2015, **137**(29), 9400–9408.
30 K. Zhu, G. M. Carignan, S. J. Teat, S. Rangan, X. Hei and L. H. Nguyen, *et al.*, Narrow Band Gap Hybrid Copper(I)Iodides: Designer Materials for Optoelectronic Applications, *Chem. Mater.*, 2024, **36**, 11139–11149.
31 D. Shi, V. Adinolfi, R. Comin, M. Yuan, E. Alarousu and A. Buin, *et al.*, Low trap-state density and long carrier diffusion in organolead trihalide perovskite single crystals, *Science*, 2015, **347**(6221), 519–522.
32 W. Ki, X. Hei, H. T. Yi, W. Liu, S. J. Teat and M. Li, *et al.*, Two-Dimensional Copper Iodide-Based Inorganic–Organic Hybrid Semiconductors: Synthesis, Structures, and Optical and Transport Properties, *Chem. Mater.*, 2021, **33**(13), 5317–5325.
33 A. V. Artem'ev, M. P. Davydova, X. Hei, M. I. Rakhmanova, D. G. Samsonenko and I. Y. Bagryanskaya, *et al.*, Family of Robust and Strongly Luminescent CuI-Based Hybrid Networks Made of Ionic and Dative Bonds, *Chem. Mater.*, 2020, **32**(24), 10708–10718.
34 T. Bai, X. Wang, Y. He, H. Wei, Y. Su and J. Chen, Turning Self-Trapped Exciton Emission to Near-Infrared Region in Thermochromism Zero-Dimensional Hybrid Metal Halides, *Adv. Opt. Mater.*, 2023, **11**(20), 2301110.
35 D. Li, H. Shi, Q. Qi, B. Chang, Y. Jiang and K. Qian, *et al.*, Clinically Translatable Solid-State Dye for NIR-II Imaging of Medical Devices, *Adv. Sci.*, 2023, **10**(36), 2303491.
36 M. Bacalum, B. Zorilă and M. Radu, Fluorescence spectra decomposition by asymmetric functions: Laurdan spectrum revisited, *Anal. Biochem.*, 2013, **440**(2), 123–129.
37 S. M. Blinder, *Introduction to quantum mechanics*, Academic Press, 2020.
38 W. Liu, Y. Fang and J. Li, Copper Iodide Based Hybrid Phosphors for Energy-Efficient General Lighting Technologies, *Adv. Funct. Mater.*, 2018, **28**(8), 1705593.
39 W. Liu, D. Banerjee, F. Lin and J. Li, Strongly luminescent inorganic–organic hybrid semiconductors with tunable white light emissions by doping, *J. Mater. Chem. C*, 2019, **7**(6), 1484–1490.
40 X. Hei, S. J. Teat, W. Liu and J. Li, Eco-friendly, solution-processable and efficient low-energy lighting phosphors:

copper halide based hybrid semiconductors Cu4X6(L)2 (X = Br, I) composed of covalent, ionic and coordinate bonds, *J. Mater. Chem. C*, 2020, **8**(47), 16790–16797.

41 A. V. Artem'ev, E. A. Pritchina, M. I. Rakhmanova, N. P. Gritsan, I. Y. Bagryanskaya and S. F. Malysheva, *et al.*, Alkyl-dependent self-assembly of the first red-emitting zwitterionic {Cu4I6} clusters from [alkyl-P(2-Py)3]+ salts and CuI: when size matters, *Dalton Trans.*, 2019, **48**(7), 2328–2337.

42 Y. Liu, A.-A. Yang, Y. Wang, W.-Z. Li, X.-S. Zhang and J. Luan, *et al.*, Synthesis of two polymorphic Cu-based coordination polymers of 1,2,4-benzenetricarboxylic acid along with a carbon-coated composite for the selective degradation of organic dyes, *J. Solid State Chem.*, 2021, **303**, 122506.

43 Z.-Y. Zhang, G.-D. Zhang, X.-X. Sheng, Q.-W. Ding, Y.-Z. Bai and Y. Su, *et al.*, Efficient MO Dye Degradation Catalyst of Cu(I)-Based Coordination Complex from Dissolution–Recrystallization Structural Transformation, *Cryst. Growth Des.*, 2021, **21**(1), 333–343.

44 D.-M. Chen, C.-X. Sun, C.-S. Liu and M. Du, Stable Layered Semiconductive Cu(I)–Organic Framework for Efficient Visible-Light-Driven Cr(VI) Reduction and H2 Evolution, *Inorg. Chem.*, 2018, **57**(13), 7975–7981.

45 X. Hei, K. Zhu, G. Carignan, S. J. Teat, M. Li and G. Zhang, *et al.*, Solution-processable copper(I) iodide-based inorganic-organic hybrid semiconductors composed of both coordinate and ionic bonds, *J. Solid State Chem.*, 2022, **314**, 123427.

46 M. Roy, A. Adhikary, A. K. Mondal and R. Mondal, Multifunctional Properties of a 1D Helical Co(II) Coordination Polymer: Toward Single-Ion Magnetic Behavior and Efficient Dye Degradation, *ACS Omega*, 2018, **3**(11), 15315–15324.

47 M. Li, F. Liu, Z. Ma, W. Liu, J. Liang and M. Tong, Different mechanisms for E. coli disinfection and BPA degradation by CeO2-AgI under visible light irradiation, *Chem. Eng. J.*, 2019, **371**, 750–758.

48 Z.-B. Wang, Y.-H. Zhang, Y.-L. Sun, M.-H. Lv, Y. Liu and W.-Z. Li, *et al.*, Pyridine-amide-based hetero-copper iodide for the photocatalytic degradation of dyes and aerosol discolouration of VOC gases, *J. Mater. Chem. C*, 2024, **12**(9), 3311–3325.

49 W. Zhang, T. Chen, P. Guo, W. Zhang and G. Yang, High removal of methyl blue over copper mixed-triazolate MOF by both adsorption and photodegradation from aqueous solution, *Microporous Mesoporous Mater.*, 2024, **369**, 113053.

50 C. X. Liu, W. H. Zhang, N. Wang, P. Guo, M. Muhler and Y. Wang, *et al.*, Highly efficient photocatalytic degradation of dyes by a copper–triazolate metal–organic framework, *Chem. – Eur. J.*, 2018, **24**(63), 16804–16813.

51 X.-S. Zhang, J.-L. Cui, Y. Liu, W.-Z. Li, Y. Liu and H. Xiang, *et al.*, Influence of anions on the synthesis of Cu (i)-based coordination polymers along with a series of derived materials for selective photocatalytic properties, *Mol. Syst. Des. Eng.*, 2023, **8**(11), 1388–1401.

52 W. Jiang, J. Li, Y. Jiang, S. Zhou, B. Liu and T. Zhou, *et al.*, A 3D porphyrinic metal-organic framework with fsc topology for efficient visible-light-driven photocatalytic degradation, *Polyhedron*, 2022, **226**, 116091.

53 A. Houas, H. Lachheb, M. Ksibi, E. Elaloui, C. Guillard and J.-M. Herrmann, Photocatalytic degradation pathway of methylene blue in water, *Appl. Catal., B*, 2001, **31**(2), 145–157.

54 I. Khan, K. Saeed, I. Zekker, B. Zhang, A. H. Hendi and A. Ahmad, *et al.*, Review on methylene blue: Its properties, uses, toxicity and photodegradation, *Water*, 2022, **14**(2), 242.

55 J. Dearden and W. Forbes, Light absorption studies: Part XIV. The ultraviolet absorption spectra of phenols, *Can. J. Chem.*, 1959, **37**(8), 1294–1304.

56 G. M. Sheldrick, Crystal structure refinement with SHELXL, *Acta Crystallogr., Sect. C: Struct, Chem*, 2015, **71**(1), 3–8.

57 P. Makuła, M. Pacia and W. Macyk, *How to correctly determine the band gap energy of modified semiconductor photocatalysts based on UV–Vis spectra*, ACS Publications, 2018. p. 6814–6817.

58 S. J. Clark, M. D. Segall, C. J. Pickard, P. J. Hasnip, M. I. J. Probert and K. Refson, *et al.*, First principles methods using CASTEP, *Z. Kristallogr. - Cryst. Mater.*, 2005, **220**(5–6), 567–570.

59 (*a*) G. M. Carignan, S. J. Teat, X. Hei, S. Chakravartula, G. Hall, L. H. Nguyen and J. Li, CCDC: 2411484: Experimental Crystal Structure Determination, 2025, DOI: **10.5517/ccdc.csd.cc2lybtq**; (*b*) G. M. Carignan, S. J. Teat, X. Hei, S. Chakravartula, G. Hall, L. H. Nguyen and J. Li, CCDC: 2411485: Experimental Crystal Structure Determination, 2025, DOI: **10.5517/ccdc.csd.cc2lybvr**; (*c*) G. M. Carignan, S. J. Teat, X. Hei, S. Chakravartula, G. Hall, L. H. Nguyen and J. Li, CCDC: 2411486: Experimental Crystal Structure Determination, 2025, DOI: **10.5517/ccdc.csd.cc2lybws**; (*d*) G. M. Carignan, S. J. Teat, X. Hei, S. Chakravartula, G. Hall, L. H. Nguyen and J. Li, CCDC: 2411487: Experimental Crystal Structure Determination, 2025, DOI: **10.5517/ccdc.csd.cc2lybxt**.

